DOI: 10.1002/asia.201300693

Reactivity of Fluoro-Substituted Bis(thiocarbonyl) Donors with Diiodine: An XRD, FT–Raman, and DFT Investigation

Annalisa Mancini,[a] M. Carla Aragoni,[a] Ann L. Bingham,[b] Carlo Castellano,[c] Susanne L. Coles (née Huth),[b] Francesco Demartin,[c] Michael B. Hursthouse,[b, d] Francesco Isaia,[a] Vito Lippolis,[a] Giuseppe Maninchedda,[a] Anna Pintus,[a] and Massimiliano Arca*[a]

Abstract: The reactions of 1,3,8,10-tetrakis(4′-fluorophenyl)-4,5,6,7-tetrathiocino[1,2-*b*:3,4-*b*′]diimidazolyl-2,9-dithione (**4**) and molecular diiodine afforded spoke adducts with stoichiometries **4**·I_2 and **4**·3I_2, isolated in the compound **4**·3I_2·$x$$CH_2Cl_2$·(1−$x$)$I_2$ (x = 0.70), and characterized by single-crystal XRD and FT–Raman spectroscopy. The nature of the reaction products was investigated under the prism of theoretical calculations carried out at the DFT level. The structural data, FT–Raman spectroscopy, and quantum mechanical calculations agree in indicating that the introduction of fluorophenyl substituents results in a lowering of the Lewis basicity of this class of bis(thiocarbonyl) donors compared with alkyl-substituted tetrathiocino donors and fluorine allows for extended interactions that are responsible for solid-state crystal packing.

Keywords: charge transfer · density functional calculations · fluorine · halogens · solid-state structures

Introduction

In recent decades, considerable interest has been focused on the reactions between chalcogenocarbonyl donors LE (L = organic framework; E = S, Se) and dihalogens XY (X, Y = Cl, Br, I),[1] owing to their implications in different fields of research, which span from synthetic to biological, materials, and industrial chemistry.[2–5] Among the most commonly encountered products obtained from such reactions,[2a,6] the following can be highlighted: 1) charge-transfer (CT) "spoke" adducts containing the linear E−X−Y group (10-X-2 hypervalent halogen compound);[1,7,8] 2) donor oxidation products with E−X terminal bonds (LEX);[8] 3) "T-shaped" hypervalent chalcogen compounds (10-E-3) L−E(X)−Y, containing an X−E−Y linear moiety;[9,10] 4) halonium species coordinated by two chalcogen donors [LE−X−EL]$^+$;[2d,11] and 5) dications containing a chalcogen–chalcogen single bond $[(LE)_2]^{2+}$.[2f,12]

We recently showed that the introduction of two C=E groups in the same substrate allowed their exploitation as versatile building blocks of supramolecular halogen-rich architectures. In fact, the capability of CT and T-shaped adducts to exploit terminal halogen/chalcogen atoms to interact with each other and with halogen units or with polyhalides, generated by oxidation of the starting chalcogen donors, makes it possible to achieve extended or even infinite polyhalogen/polyhalide networks.[7,13]

Although a serendipitous case of an infinite 2D polybromide network, obtained from the reaction of a bis(thiocarbonyl) donor, 4,5,9,10-tetrathiocino[1,2*b*:5,6-*b*′]-1,3,6,8-tetraethyldimidazolyl-2,7-dithione (**1′**), with Br_2, namely $[(\mathbf{1'}\cdot 2Br)^{2+}(Br^-)_2(Br_2)_3]$, was reported by some of the authors of this paper,[14] diiodine is the dihalogen showing the largest aptitude to form stable catenated anionic species. In fact, I_2, I^-, and I_3^- subunits can interact through I···I contacts not longer than 3.6 Å to give discrete polyiodides with the general formula $I^{n-}{}_{n+2m}$ (n, $m > 0$), such as I_4^{2-}, I_5^-, I_7^-, up to I_{29}^{3-}.[15] The aggregation of discrete polyiodides, through contacts ranging from 3.6 Å to the sum of iodine van der Waals radii (4.2 Å), can generate very intricate infinite n-dimensional networks.[16]

[a] Dr. A. Mancini, Dr. M. C. Aragoni, Prof. F. Isaia, Prof. V. Lippolis, Dr. G. Maninchedda, Dr. A. Pintus, Dr. M. Arca
Dipartimento di Scienze Chimiche e Geologiche
Università degli Studi di Cagliari
S.S. 554 bivio per Sestu
09042 Monserrato, Cagliari (Italy)
Fax: (+39) 070-675-4456
E-mail: marca@unica.it

[b] Dr. A. L. Bingham, Dr. S. L. Coles (née Huth), Prof. M. B. Hursthouse
School of Chemistry, University of Southampton
Highfield, Southampton, SO17 1BJ (UK)

[c] Dr. C. Castellano, Prof. F. Demartin
Dipartimento di Chimica
Università degli Studi di Milano
Via Golgi 19, 20133, Milano (Italy)

[d] Prof. M. B. Hursthouse
Faculty of Science, King Abdulaziz University
Jeddah, 21588 (Saudi Arabia)

Supporting information for this article is available on the WWW under http://dx.doi.org/10.1002/asia.201300693.

Recently, we reported on the products isolated from the reactions of the bis(thiocarbonyl) donors **1**–**3** (1,3,8,10-tetrasubstituted 4,5,6,7-tetrathiocino-[1,2-*b*:3,4-*b*′]-diimidazolyl-2,9-dithione; Scheme 1) with dibromine and diiodine.[10] Because the introduction of fluorine into the donor substrates could, in principle, affect both their Lewis basicity[17] and

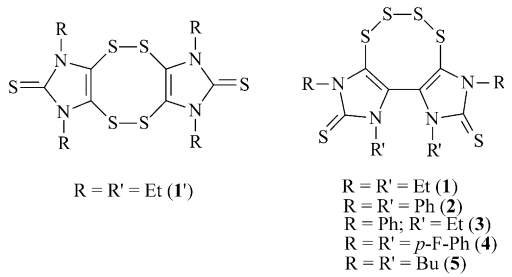

Scheme 1. Structures of compounds **1′** and **1**–**5**.

solid-state interactions in crystal packing,[18] we report herein on the reactions between 1,3,8,10-tetrakis(4′-fluorophenyl)-4,5,6,7-tetrathiocino-[1,2-*b*:3,4-*b*′]-diimidazolyl-2,9-dithione donor (**4**) and diiodine (Scheme 1).

Results and Discussion

The bis(thiocarbonyl) donor **4** was synthesized according to a modification of the procedures used for the synthesis of **1**–**3**, reported previously, from the reaction between the corresponding thioparabanic acid derivative (*N*,*N*′-disubstituted 2-thioxoimidazolidine-4,5-dione) and Lawesson's reagent (2,4-bis(4-methoxyphenyl)-1,3,2,4-dithiadiphosphetane-2,4-disulfide; Scheme S1 in the Supporting Information).[19] Compound **4** was made to react with I_2 in CH_2Cl_2 in donor/acceptor molar ratios ranging from 1:0.5 to 1:5. All isolated products were characterized by elemental analysis, FTIR spectroscopy, and FT–Raman spectroscopy, and, in the case of **4** and the products obtained from its reactions with I_2 in 1:1 and 1:5 molar ratios, also by XRD.

XRD Study

XRD analysis shows that the structural features of **4** (Figure 1) resemble closely those of previously reported tetrathiocino donors featuring phenyl substituents, such as **2** and **3**.[10,20,21] The two imidazole rings are twisted by 61.5(4)° around the C–C bond and the inner 4-fluorophenyl substituents form an angle of about 12° (intercentroid distance of 4.02 Å).

The reactions of **4** with I_2 in all molar ratios between 1:0.5 and 1:2 in CH_2Cl_2 yielded deep brown solutions, from which solid products were isolated with microanalytical data that indicated a 1:1 stoichiometry. Dark crystals were obtained by slow evaporation of the solvent, starting from a 1:1 molar ratio of **4**/I_2. These crystals were established to be **4**·I_2 by single-crystal XRD (Figure 2). Compound **4**·I_2 consists of

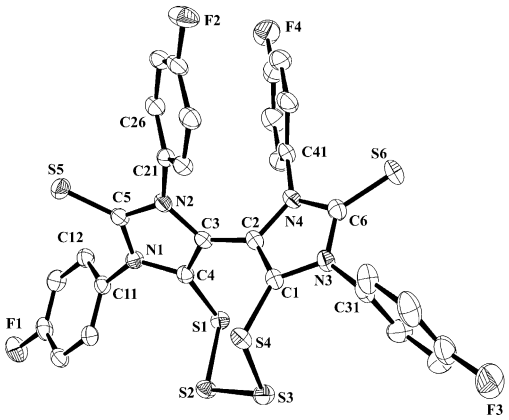

Figure 1. ORTEP drawing and atom labeling scheme for **4**. Thermal ellipsoids are shown at the 60% probability level. Hydrogen atoms are omitted for clarity. Selected distances [Å] and angles [°]: C1–N3 1.403(3), C2–N4 1.393(4), C1–C2 1.351(4), C6–N3 1.371(4), C6–N4 1.371(3), C6–S6 1.667(3), C4–N1 1.387(3), C3–N2 1.391(3), C3–C4 1.360(4), C5–N1 1.369(4), C5–N2 1.378(3), C5–S5 1.662(3), C2–C3 1.457(4); S5-C5-N1 127.3(2), S5-C5-N2 128.1(2), S6-C6-N3 127.7(2), S6-C6-N4 126.8(2), N2-C3-C2-N4 61.5(4); C12-C11-N1-C4, −82.83(4); C26-C21-N2-C3 58.8(3).

a 1:1 CT adduct that features the diiodine molecule coordinated by the sulfur atom S6 (S6–I1 = 2.736(7) Å) to give an almost linear S6–I1–I2 system. The lengthening of the donor thiocarbonyl group (C6–S6 = 1.687(16) Å) with re-

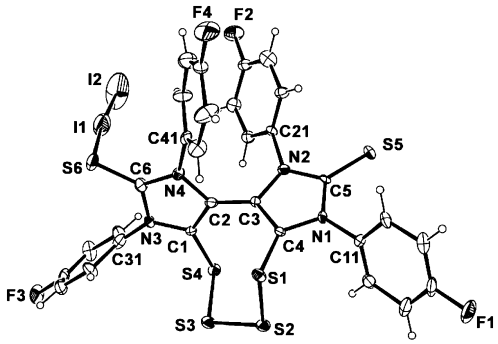

Figure 2. ORTEP drawing and atom labeling scheme for **4**·I_2. Thermal ellipsoids are shown at the 30% probability level. Selected distances [Å] and angles [°]: I1–I2 2.734(3), I1–S6 2.736(7), C6–S6 1.686(16), N3–C6 1.419(19), N4–C6 1.344(19), N3–C1 1.361(17), N4–C2 1.411(18), C1–C2 1.39(2), C2–C3 1.42(2), C3–C4 1.365(19), N2–C3 1.401(17), N1–C4 1.389(17), N2–C5 1.376(18), N1–C5 1.387(19), C5–S5 1.660(14); I2-I1-S6 175.02(13), I1-S6-C6 89.7(7), N2-C3-C2-N4 64(2).

spect to the free donor **4** (see above)[22] and the I–I bond length (I1–I2 = 2.734(3) Å; I–I distance = 2.667 and 2.714 Å in the gas phase and in the solid state, respectively)[23,24] is in agreement with a medium-strength CT interaction. Notably, the crystal structures of **1**·2I_2 and **5**·2I_2 showed that the coordinated diiodine units were elongated to a remarkably higher extent (I–I = 2.82 and 2.84 Å, respectively; **5** = 4,5,9,10-tetrathiocino-[1,2*b*:5,6-*b*′]-1,3,6,8-tetrabutyl-diimidazolyl-2,7-dithione, Scheme 1)[25] and suggested that **4** behaved as a weaker Lewis base towards I_2 as compared with **1** and **5**.

No I···I interactions below the sum of the van der Waals radii (4.2 Å) are present. Weak interactions, largely involving the terminal fluorine atoms through F···H and F···S contacts, join molecules in the solid state, with distances largely below the sum of van der Waals radii and falling in the range previously observed in similar cases (selected contacts: F2···H33^{I} 2.46(1), F4···H23^{II} 2.60(2), F3···S6^{III} = 3.19(1), I2···H43^{IV} 3.043(5) Å; ^{I} = x, 1 + y, z; ^{II} = −x, −y, 2−z; ^{III} = 1−x, −1−y, 2−z; ^{IV} = 1−x, −y, 2−z; Figure S1 in the Supporting Information). Notably, no significant interaction between the fluorine atoms and the iodine molecules, which are partially negatively charged by the CT process, occurs.

By slow evaporation of a solution containing **4** and a fivefold molar excess of diiodine in dichloromethane, crystals of the compound **4**·3I_2·$x$$CH_2Cl_2$·(1−$x$)$I_2$ (x = 0.70) were isolated and characterized by XRD (Figure 3). The crystal structure

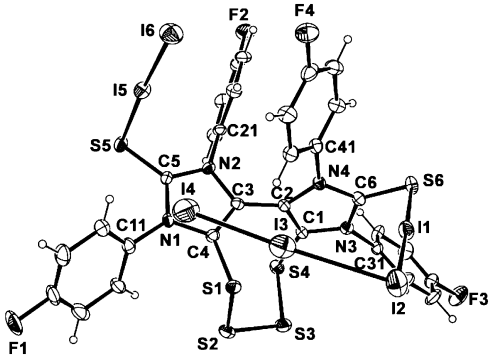

Figure 3. ORTEP drawing and atom labeling scheme for **4**·3I_2 in the compound **4**·3I_2·$x$$CH_2Cl_2$·(1−$x$)$I_2$ (x = 0.70). Thermal ellipsoids are shown at the 30% probability level. Selected distances [Å] and angles [°]: C6−S6 1.690(9), C5−S5 1.705(9), S5−I5 2.814(3), S6−I1 2.692(3), I5−I6 2.8195(12), I1−I2 2.9137(13), I2···I3 3.182(2), I3−I4 2.7391(17); C6-S6-I1 93.5(3), S6-I1-I2 178.03(7), I1-I2-I3 92.04(4), I2-I3-I4 175.07(6), C5-S5-I5 91.3(3), S5-I5-I6 176.57(6), N2-C3-C2-N4 78.1(1).

shows two diiodine molecules linearly bonded to the exocyclic sulfur atoms S5 and S6 and perpendicular to the planes of the relevant imidazolidine rings. A third diiodine molecule interacts with I1−I2 and results in a slight elongation (I3−I4 2.738(2) Å) with respect to uncoordinated I_2. The I2···I3 distance is remarkably short (3.182(2) Å) relative to that found in different poly(diiodine) complexes.[26] Thus, the moiety I1−I2···I3−I4 can be identified as an "L-shaped" I_4 neutral system, which is closely related to those characterized in the products obtained from the reactions between imidazolidine-2-thione[27] and *N*-methylbenzothiazole-2-(3*H*)selone[28] with I_2, featuring a LSe···I_2···I_2 system with all I−I distances below 3.4 Å. As a further example of a recently reported polyiodine system, compound **6**·2.5I_2 (**6** = 4,5-bis(-benzoylthio)-1,3-dithiole-2-thione) can be mentioned, in which different S-coordinated I_2 units are bridged by diiodine molecules with I···I interactions of 3.464(22) and 3.497(24) Å to form a sequence of 12 iodine atoms.[7]

In the crystal packing of **4**·3I_2·$x$$CH_2Cl_2$·(1−$x$)$I_2$ (x = 0.70), clathrated molecules of dichloromethane and diiodine (I7−I8, not represented in Figure 3) are statistically distributed with a 0.70:0.30 molar ratio of CH_2Cl_2/I_2. The pattern of crystal packing is mainly controlled by long interactions that separately involve both iodine and fluorine atoms (selected contacts: I2···I3 3.182(2), F1···H32^{I} = 2.60(1), F4···H23^{II} = 2.48(1), I4···I8 = 3.934(7), I6···I8 = 3.907(5), I2···I7^{III} = 3.942(3), I4···S4^{IV} = 3.738(3), I6···H26^{IV} 3.074(1), I7···H13 3.149(4) Å; ^{I} = 1−x, 2−y, −z; ^{II} = 1−x, 3−y, 1−z; ^{III} = −x, 2−y, −z; ^{IV} = −1 + x, y, z; Figure S2 in the Supporting Information).

The capability of diiodine units S-coordinated by tetrathiocino donors to further act as Lewis bases, as found in **4**·3I_2·$x$$CH_2Cl_2$·(1−$x$)$I_2$ (x = 0.70), was also demonstrated recently in the case of donor **3**, the reactions of which with I_2 resulted in the formation of the compounds **3**·2I_2·(1−x)·$x$$CH_2Cl_2$ (x = 0.94) and (**3**)$_2$·7I_2·$x$$CH_2Cl_2$ (x=0.66).[10]

Recently,[29] we demonstrated that three-body fragments A-B-C, such as E-X-Y, X-E-Y, and E-X-E (E = chalcogen; X, Y = halogen species) feature a common correlation between the two distances A−B and B−C. In fact, experimental data can be fitted according to an approximate relationship derived from the bond-valence model.[30] In particular, in the case of systems S···I−I (A = S; B = C = I), the correlation given by Equation (1) can be applied:

$$\delta_1 = -k \ln\left[1 - e^{-\frac{\delta_2}{k}}\right] \tag{1}$$

in which δ_1 and δ_2 represent elongations of the I−I and S···I distances, which are normalized with respect to the sum of the covalent radii of the atomic species involved r_S and r_I, given by Equation (2):

$$\delta_1 = \frac{d_{I-I} - 2r_I}{2r_I} \text{ and } \delta_2 = \frac{d_{S\cdots I} - (r_S + r_I)}{r_S + r_I} \tag{2}$$

Analysis of the δ_1/δ_2 couples provided by the structural data of the few related CT adducts that feature the S···I−I three-body systems (Table 1) shows that I−I and S···I distances fall within the same correlation shared by the three-body systems analyzed previously (Figure 4; k = 0.161; root-mean-square deviation (RMSD) = 3.66×10^{-3}). Notably, only the δ_1/δ_2 couple of the adduct **4**·I_2 represents an anomaly with respect to all the other CT adducts derived from tetrathiocino donors **1**–**5**; this is possibly because of the quality of the structure refinement, as reflected in rather large standard deviation values for the S−I and I−I distances.

Quantum Mechanical Calculations

During recent years, theoretical calculations based on DFT have been exploited largely to investigate the nature and mechanistic aspects that lead to the final products obtained from the reactions between various types of chalcogen donors and dihalogens/interhalogens.[2f,31–34] In this context, we have underlined that the natural charge distribution on

Table 1. Structural I–I, S···I, and C=S distances (d_{I-I}, $d_{S\cdots I}$, and d_{C-S}, respectively; Å) of the fragments C=S···I–I and FT–Raman response ν [cm^{-1}] for the CT adducts obtained from donors **1**–**5**.

	x	d_{I-I}	$d_{S\cdots I}$	$d_{C=S}$	ν
1·$2I_2$		2.822(2)	2.775(4)	1.70(1)	146[a,b]
2·I_2		–	–	–	134[a]
2·$2I_2$		–	–	–	171[a]
					113[c]
2·$2I_2$·$2CHCl_3$		–	–	–	172[d]
					114[c]
3·$2I_2$·xCH_2Cl_2· $(1-x)I_2$	0.94	2.8931(4)	2.677(29)	1.719(2)	137[a]
		2.8392(3)	2.7441(9)	1.697(3)	
$(\mathbf{3})_2$·$7I_2$·xCH_2Cl_2	0.66	2.9120(6)	2.649(1)	1.683(5)	146[a]
		2.8933(7)	2.673(2)	1.696(6)	
		2.7502(8)	–	–	175
		2.7343(7)	–	–	
4·I_2		2.734(3)	2.736(7)	1.686(17)	–
4·$3I_2$·xCH_2Cl_2·$(1-x)I_2$	0.70	2.9137(13)	2.692(3)	1.690(9)	127[e]
		2.8195(12)	2.814(3)	1.705(9)	144
		2.7391(17)	–	–	170
5·$2I_2$		2.840(2)	2.783(5)	1.69(2)	152[b]

[a] Ref. [10]. [b] Ref. [25]. [c] Attributed to linear symmetric I_3^-, which was possibly generated by laser decomposition. [d] Ref. [41]. [e] This work.

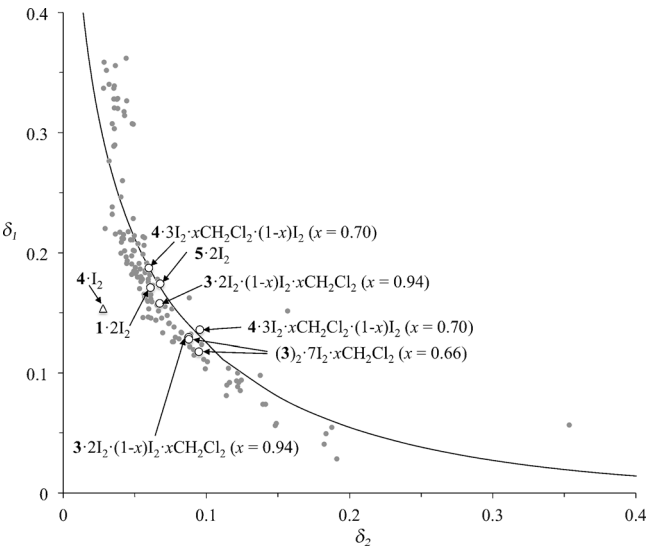

Figure 4. Fitting of the δ_1 and δ_2 structural parameters [Eq. (2)] for the S-I-I three-body systems in CT adducts characterized structurally. Structural data reported herein are shown as open symbols and data retrieved from the CCDC as dots. The solid curve represents the least-squares fit of all data by adopting Equation (1) as a model ($k=0.161$; RMSD 3.66×10^{-3}). The data for the entry XOVRIJ,[2d] represented by a filled rhombus, and that of **4**·I_2 (open triangle) have been considered as anomalies and have not been included in the fitted data.

the hypothetical intermediate cationic species $[LEX]^+$ (L = organic framework; E = S, Se; X = I, Br), which is in principle derived from the heterolytic breaking of either the X–X or E–X bonds of CT or T-shaped adducts, respectively, represents a useful tool to predict correctly the outcome of the reactions between LE donors and halogens X_2 or interhalogens XY.[31,32,35]

Previously, several papers have dealt with the theoretical characterization of CT adduct formation between thio- and selenocarbonyl donors and I_2. In particular, we reported an experimental and theoretical investigation of the nature of the 1:1 and 1:2 CT adducts formed between neutral bis(1,2-dithiolene) complexes [M(R,R′timdt)$_2$] (M = Ni, Pd, Pt; R,R′timdt = formally monoreduced *N*,*N*′-disubstituted imidazolidine-2,4,5-trithione), which are a class of bis(thiocarbonyl) donors.[31] With the aim of understanding the nature of the products obtained in the particular case of the title bis(thiocarbonyl) donors with diiodine, and to find out the effect of the interaction of a single C=S group with I_2 on the donor ability of the second one, hybrid DFT calculations were carried out on **4**, **4**·I_2, and related species. Three different density functionals were tested for the title systems, namely, the well-known three-parameters B3LYP;[36] Adamo and Barone's mPW1PW,[37] and the functional B97D,[38] which was chosen to account for dispersion effects. Selected metric parameters optimized for **4**·I_2 are summarized in Table 2. A comparison with the corresponding structural parameters determined by XRD (Figure 2) reveals very good agreement, although the C–S bond length of the thiocarbonyl group is slightly underestimated and S–I distances are overestimated. In agreement with what was previously reported in the case of the T-shaped adduct formed between 4,5-bis(benzoylthio)-1,3-dithiole-2-thione and molecular bromine,[7] the mPW1PW functional provides the best agreement, especially as far as the distances within the >C=S···I–I fragments are regarded, and was therefore adopted for all calculations carried out on related systems.

Table 2. Selected bond lengths [Å], angles [°], and dihedral angles [°] optimized at the DFT level for **4**·I_2 (atoms are labeled by following the numbering scheme reported in Figure 2).

	B3LYP	mPW1PW	B97D
I1–I2	2.840	2.801	2.887
I1–S6	2.983	2.924	2.965
C5–S5	1.655	1.649	1.657
C6–S6	1.692	1.684	1.695
I2-I1-S6	178.94	178.68	175.09
C6-S6-I1	98.15	96.88	92.22

The calculated Kohn–Sham (KS) HOMO (Figure 5a) and KS-HOMO-1 calculated for **4** at the optimized geometry[39] are constituted by the in-phase and out-of-phase combinations of the lone pairs (LPs) located on the terminal sulfur atoms of the thiocarbonyl groups, which are disposed perpendicularly to the imidazole plane. Phenyl substituents render the terminal sulfur atoms less negatively charged than those of alkyl-substituted analogues (natural charge $Q_S = -0.258$, -0.191, and $-0.195\,e$ for **1**, **2**, and **4**,[40] respectively); this is in agreement with the structural features of **4**·I_2 and **1**·$2I_2$ discussed above and FT–Raman measurements carried out on the compound **2**·$2I_2$·$2CHCl_3$.[41] Notably, a comparison of the natural charges Q_S calculated for **2** and **4** shows that no direct effect is achieved as a consequence of the fluorination of the phenyl substituents.

A molecular orbital analysis of the hypothetical cation $[\mathbf{4}\cdot I]^+$ shows that the composition of the KS-LUMO (Fig-

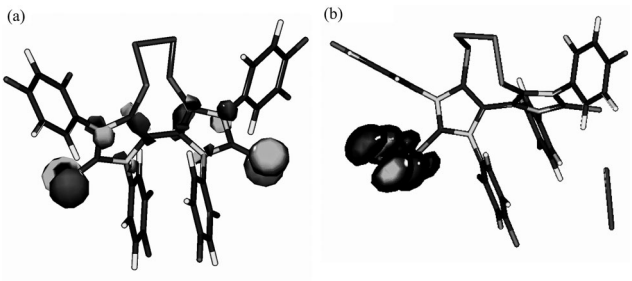

Figure 5. Isosurface of the KS-HOMOs calculated for **4** (a) and **4**•I_2 (b). Contour plot 0.05 *e*.

ure S3 in the Supporting Information) and the positive natural charge[42] on the terminal I atom ($Q_S = +0.098\,e$; $Q_I = +0.138\,e$) support only the formation of the CT-type adduct **4**•I_2. The CT σ-interaction (net natural charge transfer = 0.253 *e*) between the donor LPs and the diiodine LUMO induces a lengthening of the I–I distance (calculated I–I distance = 2.685 and 2.802 Å in free I_2 and **4**•I_2, respectively), which is reflected in a lowering of the corresponding Wiberg bond index with respect to the free components (WBI_{I1-I2} = 1.02 and 0.755 in I_2 and **4**•I_2, respectively; WBI_{C6-S6} = 1.585 and 1.684 for **4** and **4**•I_2, respectively). Notably, the free thiocarbonyl group is only marginally perturbed by the formation of the adduct (C5–S5 = 1.649 Å; $Q_{S5} = -0.179\,e$; WBI_{C5-S5} = 1.595), and it is therefore available to further interact with a second unit of I_2 to give adducts with higher molar iodine content, such as that found in the case of **4**•3I_2•$x$$CH_2Cl_2$•$(1-x)I_2$ (x = 0.70). Accordingly, the KS-HOMO and KS-HOMO-1 calculated for the hypothetical 1:2 CT adduct **4**•2I_2 are largely localized on the negatively charged terminal iodine atoms (Figure 5b; average natural charge[43] on terminal iodine $Q_I = -0.190\,e$), which are in turn capable of acting as donors towards further diiodine molecules.

The geometry of compound **4**•3I_2 has been also optimized by starting from the structural data for compound **4**•3I_2•$x$$CH_2Cl_2$•$(1-x)I_2$ (x = 0.70). Notably, the pattern of the I–I bond lengths within this compound is correctly reproduced in the optimized geometry, with I1–I2 > I5–I6 > I3–I4 (2.914, 2.819, and 2.781 Å, respectively; I3-I2-I1 89.29°). In fact, in agreement with the structural features discussed above for compound **4**•3I_2•$x$$CH_2Cl_2$•$(1-x)I_2$ (x = 0.70), the diiodine I1–I2, which bridges the C6–S6 donor group and the I3–I4 unit, is the most elongated dihalogen unit, whereas I3–I4 features the shortest bond length. Accordingly, the corresponding WBI[44] can be strictly correlated with the experimental bond lengths (R^2 = 0.98). The interaction between the I1–I2 unit and I3–I4 (optimized I2···I3 distance 3.233 Å) is reflected in a $WBI_{I2\cdots I3}$ value of 0.237. The optimized structure calculated at the same level of theory for the L-shaped I_4 system shows the two diiodine units at a longer distance (3.556 Å) and forming an I–I···I angle of 106.27°, with a WBI between the interacting iodine atoms of the two units of 0.085. This suggests that the CT process from donor **4** to the I1–I2 unit is essential in stabilizing the I1–I2···I3–I4 moiety.

It is worth noting that the terminal iodine atoms I4 and I6 in **4**•3I_2 feature similar negative natural charges (−0.180 and −0.187 *e*, respectively) and are therefore available to participate in further CT interactions, as testified by the non-stoichiometric iodine content in the compound **4**•3I_2•$x$$CH_2Cl_2$•$(1-x)I_2$ (x = 0.70).

FT–Raman Spectroscopy

Low-frequency FT–Raman spectroscopy (50–500 cm^{-1}) is a powerful tool to detect the formation of halogen-bonded adducts.[10,45,46] In the case of diiodine adducts, FT–Raman spectroscopy has been shown to give reliable information on the elongation of the I–I bond length in perturbed diiodine molecules with respect to that measured in the free dihalogen. Although fluorescence and/or fast decomposition induced by laser irradiation made it difficult to record a good quality spectrum for **4**•I_2, the FT–Raman spectrum of **4**•3I_2•$x$$CH_2Cl_2$•$(1-x)I_2$ (x = 0.70; Figure S4 in the Supporting Information) was in good agreement with the structural features discussed above. In the FT–Raman spectrum a broad structured peak, with a maximum at 170 cm^{-1} and a shoulder at 188 cm^{-1} (see the Supporting Information; relative intensities 8.9 and 10.0), can be observed, with two peaks at lower energy falling at 144 and 127 cm^{-1} (relative intensities 8.1 and 8.4, respectively). The excellent agreement between the optimized metric parameters of **4**•3I_2 and the structural features of the same adduct characterized in **4**•3I_2•$x$$CH_2Cl_2$•$(1-x)I_2$ (x = 0.70) suggested the possibility of exploiting vibrational frequency calculations to investigate the experimental FT–Raman spectrum. The Raman spectrum simulated on the basis of the scaled[47] calculated Raman-active harmonic frequencies with the PyFreq program (Figure S5 in the Supporting Information) featured a well-defined maximum, calculated to fall at 131 cm^{-1} (Raman intensity 51.2 $Å^4$/amu), which was mainly due to stretching of the I1–I2 unit, and a broad peak that resulted from the overlap of three harmonic frequencies with similar energies (159.6, 160.8, and 163.9 cm^{-1}; Raman intensity 91.8, 57.2, and 47.7 $Å^4$/amu, respectively), owing to stretching vibrations of the I5–I6 and I3–I4 molecules coupled with the torsion of the C_4S_4 tetrathiocino ring and librations of the aromatic substituents. Hence, the experimental FT–Raman spectrum clearly reflects the order of the perturbation of the diiodine units in **4**•3I_2•$x$$CH_2Cl_2$•$(1-x)I_2$ (x = 0.70), that is, I1–I2 (2.9137(13) Å, 127 cm^{-1}), I5–I6 (2.8195(12) Å, 144 cm^{-1}), and I3–I4 (2.7391(17) Å, 170 cm^{-1}), whereas the shoulder at 188 cm^{-1} can be attributed to the almost unperturbed non-stoichiometric amount of diiodine cocrystallized in **4**•3I_2•$x$$CH_2Cl_2$•$(1-x)I_2$ (x = 0.70). It is worth noting that the FT–Raman spectrum collected for **4**•3I_2•$x$$CH_2Cl_2$•$(1-x)I_2$ (x = 0.70) falls within the framework of spectral data reported so far for all CT adducts derived from donors **1–5** (Table 1), showing a roughly linear correlation between the I–I distance of the perturbed diiodine units and their FT–

Raman response; this is in agreement with what was previously observed for different medium–weak CT adducts formed between chalcogen donors and I_2.[48]

Conclusion

The reactivity of the fluorosubstituted tetrathiocino donor **4** towards I_2 was investigated through a combined approach based on single-crystal XRD and FT–Raman spectroscopy. The reactions between the bis(thiocarbonyl) donor and the dihalogen, depending upon the starting molar ratios **4**/I_2, led to spoke CT adducts. The formation of the adducts could be ascribed to CT from the upper-most filled molecular orbitals of the donors (HOMO and HOMO-1, which were localized on the terminal S atoms of the thiocarbonyl groups and disposed perpendicularly to the imidazole plane) to the antibonding LUMO of the dihalogen.

The CT adducts themselves showed donor ability through their terminal iodine atoms, which resulted in the possibility of forming products with complex stoichiometry, such as **4**·3 I_2·$x$$CH_2Cl_2$·(1−$x$)$I_2$ (x=0.70), and the previously reported compounds **3**·2 I_2(1−x)I_2·$x$$CH_2Cl_2$ (x=0.94) and (**3**)$_2$·7 I_2·$x$$CH_2Cl_2$ (x=0.66).[10]

The effect of the introduction of fluorine at the phenyl substituents did not result in direct modification of the donor ability of the title class of bis(thiocarbonyl) donors towards diiodine. Conversely, natural bond orbital (NBO) calculations clearly indicated that the Lewis basicity of donor **4** was lower than that of alkyl-substituted species, such as **1**, owing to the presence of phenyl substituents, whereas on passing from **2** to **4** no remarkable effect was predicted.

Accordingly, the I–I bond length of the coordinated diiodine unit in **4**·I_2 was elongated to a lesser extent than that found in the case of CT adducts of related donors that featured alkyl substituents, such as **1**·2 I_2 and **5**·2 I_2.

On the other hand, the fluorine atoms of the 4-fluorophenyl substituents participated in F···S and F···H interactions that were co-responsible for crystal packing of the isolated compounds. Such interactions represent a further tool in the crystal engineering of ordered solid-state phases of compounds with a high content in halogen species, thus suggesting that fluoro-substituted donors could represent promising building blocks for solid-state halogen harvesting and storage based on CT interactions.

Experimental Section

General

All solvents and reagents were purchased from Aldrich and used without further purification. Elemental analyses were performed on a FISONS EA-1108 CHNS-O instrument. IR spectra were recorded on a Bruker IFS55 spectrometer at room temperature, after purging the sample cell with a flow of dried air. Polythene pellets with a Mylar beam-splitter and polythene windows (500–50 cm^{-1}, resolution 2 cm^{-1}) and KBr pellets with a KBr beam-splitter and KBr windows (4000–400 cm^{-1}, resolution 4 cm^{-1}) were used. FT–Raman spectra, in the range 500–50 cm^{-1}, were recorded with a resolution of 2 cm^{-1} on a Bruker RFS100 FT–Raman spectrometer, fitted with an In–Ga–As detector (room temperature) operating with a Nd-YAG laser (excitation wavelength 1064 nm; 100 mW), with a 180° scattering geometry.

X-ray Crystallography

A summary of the crystal data and refinement details for compounds **4**, **4**·I_2, and **4**·3 I_2·$x$$CH_2Cl_2$·(1−$x$)$I_2$ (x=0.70) is given in the Analytical Data section below. Intensity data for **4** were collected on a Bruker Nonius rotating anode KappaCCD area detector diffractometer by using confocal mirrors and MoKα radiation (ϕ scans and ω scans) at 120(2) K. Data were corrected for absorption effects with the SO RTAV software.[49] The structure was solved and refined by using the SHELX program. The structure contained some disordered solvent, which could not be modeled satisfactorily. This contribution was hence removed by using Platon/SQUEEZE. Intensity data for **4**·I_2, and **4**·3 I_2·$x$$CH_2Cl_2$·(1−$x$)$I_2$ (x=0.70) were collected at room temperature on a BrukerSmart CCD diffractometer by using graphite-monochromatized MoKα radiation (λ=0.71073 Å). Datasets were corrected for Lorentz polarization effects and for absorption (SADABS[50]). All structures were solved by direct methods (SIR-97[51]) and completed by iterative cycles of full-matrix least squares refinement on F_o^2 and ΔF synthesis by using the SHELXL-97[52] program (WinGX suite).[53] Hydrogen atoms, which were located on the ΔF maps, with the exception of those of the clathrated solvent molecules, were allowed to ride on their carbon atoms. In the case of **4**·I_2, several peaks of about 1.5 e $Å^{-3}$ were observed in the final difference-Fourier map, owing to the presence of disordered solvent molecules trapped in the crystal. However, no reliable disorder models could be obtained, and thus, the high value of the final R index in the structure refinement could be explained. For **4**·3 I_2·$x$$CH_2Cl_2$·(1−$x$)$I_2$ (x=0.70), the occupancy of the clathrated CH_2Cl_2 molecules was refined. The values obtained for the latter compounds showed that the cages occupied by these molecules contained also statistically distributed diiodine molecules, which almost exactly overlapped with the position of the chlorine atoms. By taking into account that the steric hindrance of a CH_2Cl_2 molecule was similar to that of a diiodine molecule, and that the Cl···Cl distance was comparable to the I–I bond length, this result was not unexpected.

CCDC 937822 (**4**), 937824 (**4**·I_2), and 937823 (**4**·3 I_2·$x$$CH_2Cl_2$·(1−$x$)$I_2$ (x=0.70; excluding structure factors)) contains the supplementary crystallographic data for this paper. These data can be obtained free of charge from The Cambridge Crystallographic Data Centre via www.ccdc.cam.ac.uk/data_request/cif.

DFT Calculations

DFT calculations were performed on **1**, **1**·2 I_2, **2**, **4**, [**4**·I]$^+$, **4**·I_2, and **4**·2 I_2, and **4**·3 I_2 with the commercial suite of Gaussian 09 software.[54] All calculations were carried out with the mPW1PW hybrid functional[36] (see discussion). The full-electron Ahlrichs pVDZ basis sets[55] were exploited for C, H, O, N, S, and F atoms and the LANL08(d) basis set with effective core potentials (ECP)[56] was used for iodine. NBO populations[57] and WBIs[58] were calculated at the optimized geometries, which were verified by harmonic frequency calculations. The results of the calculations were examined with the GaussView 5[59] and Molden 5.0[60] programs. To analyze vibrational spectral data and to simulate the corresponding Raman spectra, the program PyFreq was developed.[61] PyFreq extracts the vibrational information from Gaussian output files (frequencies, Raman activities, IR intensities), evidences and lists imaginary frequencies, and allows the vibrational spectra to be plotted as sums of Gaussian-shaped peaks centered at the scaled calculated frequencies. PyFreq is a cross-platform program developed with Python 2.7 and PyGame.

Synthesis

Compound **4** was prepared according to literature methods by treating *N*,*N*′-bis(4′-fluorophenyl)imidazolidine-2-thione-4,5-dione (2.00 g, 6.29×10^{-3} mol) with Lawesson's reagent[19] (2.60 g, 6.43×10^{-3} mol) in toluene (100 mL) and heating the reaction mixture under reflux for 2 h (Scheme S1 in the Supporting Information). The solvent was removed

under reduced pressure and an analytically pure sample was obtained by recrystallization from ethyl alcohol (yield: 26%). The reactions between **4** and I_2 were carried out according to the following procedure: a solution (30 mL of CH_2Cl_2) of a weighed amount of **4** (100 mg, 1.43×10^{-4} mol) was made to react with a solution of I_2 in 1:1 and 1:5 molar ratios (36.3 mg, 1.43 10^{-4} mol for **4**·I_2 and 0.18 g, 7.15 10^{-4} mol for **4**·$3I_2$·xCH_2Cl_2·$(1-x)I_2$ ($x=0.70$)). The solution was allowed to slowly evaporate in air. After a few days, crystals of **4**·I_2 and **4**·$3I_2$·xCH_2Cl_2·$(1-x)I_2$ ($x=0.70$) were harvested by filtration and washed with a small quantity of petroleum ether (b.p. 40–60 °C). Solid-state FTIR (4000–500 cm^{-1}, KBr pellet): $\tilde{\nu}=3117$ (m), 3074 (s), 3060 (s), 1892 (w), 1617 (s), 1598 (s), 1508 (s), 1420 (m), 1373 (s), 1325 (s), 1289 (s), 1220 (s), 1154 (s), 1095 (m), 1070 (m), 1012 (m), 936 (w), 901 (m), 839 (s), 816 (m), 758 (m), 730 (s), 708 (m), 623 cm^{-1} (m); (500–50 cm^{-1}, polythene pellet): $\tilde{\nu}=533$ (w), 517 (m), 465 (s), 444 (m), 412 (s), 390 (w), 357 (m), 315 (w), 274 (w), 237 cm^{-1} (m); FT–Raman (solid in capillary tube, 50 mW): $\tilde{\nu}$ (%) = 484.0 (28), 433.1 (54), 408.5 (18), 391.9 (24), 343.4 (16), 254.4 (17), 229.8 (27), 206.3 (21), 175.1 (20), 155.8 (23), 141.5 (36), 126.5 (51), 110.2 (100), 84.1 cm^{-1} (50); elemental analysis calcd (%) for $C_{30}H_{16}F_4N_4S_6$: C 51.41, H 2.30, N 7.99, S 27.45; found C 50.91, H 1.85, N 7.56, S 27.48.

Crystal data for **4**: $C_{30}H_{16}F_4N_4S_6$; $M_w=700.83$; monoclinic; space group $P2_1/c$; $a=11.2609(14)$, $b=24.001(4)$, $c=13.144(2)$ Å; $\alpha=90.00$, $\beta=113.540(13)$, $\gamma=90.00°$; $V=3256.8(9)$ Å^3; $Z=4$; $\rho_{calcd}=1.429$ Mg m^{-3}; $T=120(2)$ K; 27908 reflections measured; 7093 unique reflections ($R_{int}=0.058$); R_1 (observed data) = 0.0522 and wR_2 (all data) = 0.1456.

*Analytical Data for **4**·I_2*

Solid-state FTIR (4000–500 cm^{-1}, KBr pellet): $\tilde{\nu}=3550$ (m), 3060 (m), 3048 (m), 3030 (m), 1750 (m), 1875 (m), 1600 (m), 1552 (w), 1502 (s), 1420 (m), 1375 (m), 1360 (m), 1325 (s), 1290 (m), 1225 (s), 1160 (m), 1114 (m), 1020 (w), 1010 (w), 840 (s), 762 (m), 730 (m), 710 (m), 690 (w), 640 (w), 630 (w), 575 (m), 532 (m); (500–50 cm^{-1}, polythene pellet): $\tilde{\nu}=468$ (m), 448 (m), 422 (m), 398 (m), 350 (s), 346 (w), 330 (m), 320 (m), 300 (m), 286 (m), 252 (s), 220 (m), 200 (s), 196 cm^{-1} (m); elemental analysis calcd (%) for $C_{30}H_{16}F_4N_4S_6I_2$: C 37.74, H 1.69, N 5.87, S 20.14; found: C 37.58, H 1.72, N 6.18, S 20.36.

Crystal data: $C_{30}H_{16}N_4F_4S_6I_2$; $M_w=954.69$; triclinic; space group $P\bar{1}$; $a=11.333(1)$, $b=13.320(1)$, $c=13.611(1)$ Å; $\alpha=96.93(1)$, $\beta=110.19(1)$, $\gamma=111.63(1)°$; $V=1718.7(2)$ Å^3; $Z=2$; $\rho_{calcd}=1.845$ Mg m^{-3}; $T=293(2)$ K; 19117 reflections measured; 6721 unique reflections ($R_{int}=0.037$); R_1 (observed data) = 0.1333 and wR_2 (all data) = 0.4116.

*Analytical Data for **4**·3 I_2·xCH_2Cl_2·$(1-x)I_2$ ($x=0.70$)*

Solid-state FTIR (4000–500 cm^{-1}, KBr pellet): $\tilde{\nu}=3010$ (m), 2350 (m), 1600 (m), 1502 (s), 1485 (w), 1475 (w), 1450 (w), 1418 (m), 1390 (w), 1385 (m), 1380 (s), 1290 (m), 1160 (m), 1090 (m), 846 (s), 842 (w), 486 (m), 450 (m), 435 (w), 408 (m); (500–50 cm^{-1}, polythene pellet): $\tilde{\nu}=392$ (w), 356 (m), 225 (m), 210 (m), 190 (m), 180 (m) cm^{-1}; FT–Raman (solid in capillary tube, 50 mW; Figure S2 in the Supporting Information): $\tilde{\nu}$ (%) = 228.5 (25), 187.6 (89), 170.0 (100), 144.2 (81), 127.3 (84), 83.6 (31), 63.4 (16); elemental analysis calcd (%) for $C_{30.70}H_{17.40}F_4N_4S_6I_{6.60}Cl_{1.40}$: C 23.08, H 1.10, N 3.51, S 12.04; found: C 22.88, H 0.89, N 3.47, S 11.96.

Crystal data: $C_{30.70}H_{17.40}F_4N_4S_6I_{6.60}Cl_{1.40}$; $M_w=1597.82$; triclinic; space group $P\bar{1}$; $a=11.1942(9)$, $b=13.0498(11)$, $c=17.7233(14)$ Å; $\alpha=100.96(1)$, $\beta=95.72(1)$, $\gamma=114.79(1)°$; $V=2260.4(3)$ Å^3; $Z=2$; $\rho_{calcd}=2.348$ Mg m^{-3}; $T=294(2)$ K; 21011 reflections measured; 6721 unique reflections ($R_{int}=0.022$); R_1 (observed data) = 0.0656 and wR_2 (all data) = 0.2056.

Acknowledgements

A.M. acknowledges the Regione Autonoma della Sardegna (L.R. 7/2007) for financial support.

[1] a) Y. Mutoh, N. Kozono, K. Ikenaga, Y. Ishii, *Coord. Chem. Rev.* **2012**, *256*, 589–605; b) N. Kuhn, G. Verani in *Handbook of Chalcogen Chemistry: New Perspective in Sulfur, Selenium and Tellurium* (Ed.: F. A. Devillanova), RSC Publishing, Cambridge, **2007**, Chap. 2.3, pp. 107–144.

[2] a) P. D. Boyle, S. M. Godfrey, *Coord. Chem. Rev.* **2001**, *223*, 265–299; b) D. W. Allen, R. Berridge, N. Bricklebank, S. D. Forder, F. Palacio, S. J. Coles, M. B. Hursthouse, P. J. Skabara, *Inorg. Chem.* **2003**, *42*, 3975–3977; c) C. D. Antoniadis, G. J. Corban, S. K. Hadjikakou, N. Hadjiliadis, M. Kubicki, S. Warner, I. S. Butler, *Eur. J. Inorg. Chem.* **2003**, 1635–1640; d) V. Daga, S. K. Hadjikakou, N. Hadjiliadis, M. Kubick, J. H. Z. Santos, I. S. Butler, *Eur. J. Inorg. Chem.* **2002**, 1718–1728; e) M. C. Aragoni, M. Arca, F. Demartin, F. A. Devillanova, A. Garau, F. Isaia, V. Lippolis, G. Verani, *J. Am. Chem. Soc.* **2002**, *124*, 4538–4539; f) J. Konu, T. Chivers, H. M. Tuononen, *Chem. Eur. J.* **2010**, *16*, 12977–12987.

[3] a) S. W. Chu, S. J. Baek, D. C. Kim, S. Seo, J. S. Kim, Y. W. Park, *Synth. Met.* **2012**, *162*, 1689–1693; b) T. Hasell, M. Schmidtmann, A. I. Cooper, *J. Am. Chem. Soc.* **2011**, *133*, 14920–14923; c) J. R. Ferraro, J. M. Williams, *Introduction to Synthetic Electrical Conductors*, Academic Press, New York, **1987**.

[4] a) M. C. Aragoni, M. Arca, M. B. Carrea, F. Demartin, F. A. Devillanova, A. Garau, F. Isaia, V. Lippolis, G. Verani, *Eur. J. Inorg. Chem.* **2004**, 4660–4668; b) F. Isaia, M. C. Aragoni, M. Arca, C. Caltagirone, C. Castellano, F. Demartin, A. Garau, V. Lippolis, A. Pintus, *Dalton Trans.* **2011**, *40*, 4505–4513.

[5] F. Isaia, M. C. Aragoni, M. Arca, C. Caltagirone, F. Demartin, A. Garau, V. Lippolis, *Dalton Trans.* **2013**, *42*, 492–498.

[6] M. C. Aragoni, M. Arca, F. Demartin, F. A. Devillanova, A. Garau, F. Isaia, F. Lelj, V. Lippolis, G. Verani, *Chem. Eur. J.* **2001**, *7*, 3122–3133.

[7] A. Mancini, L. Pala, M. C. Aragoni, M. Arca, F. A. Devillanova, M. B. H. Hursthouse, M. E. Light, P. J. Skabara, N. Bricklebank, *Eur. J. Inorg. Chem.* **2012**, 2373–2380.

[8] P. J. Skabara, N. Bricklebank, R. Berridge, S. Long, M. E. Light, S. J. Coles, M. B. Hursthouse, *J. Chem. Soc. Dalton Trans.* **2000**, 3235–3236.

[9] P. J. Skabara, N. Bricklebank, D. E. Hibbs, M. B. Hursthouse, K. M. A. Malik, *J. Chem. Soc. Dalton Trans.* **1999**, 3007–3014.

[10] A. Mancini, M. C. Aragoni, N. Bricklebank, C. Castellano, F. Demartin, F. Isaia, V. Lippolis, A. Pintus, M. Arca, *Chem. Asian J.* **2012**, *7*, 639–647.

[11] F. Demartin, F. A. Devillanova, F. Isaia, V. Lippolis, G. Verani, *Inorg. Chem.* **1993**, *32*, 3694–3699.

[12] A. J. Blake, F. A. Devillanova, R. O. Gould, V. Lippolis, S. Parsons, C. Radek, M. Schröder, *Chem. Soc. Rev.* **1998**, *27*, 195–206.

[13] M. C. Aragoni, M. Arca, A. J. Blake, F. A. Devillanova, W.-W. du Mont, A. Garau, F. Isaia, V. Lippolis, G. Verani, C. Wilson, *Angew. Chem.* **2001**, *113*, 4359–4362; *Angew. Chem. Int. Ed.* **2001**, *40*, 4229–4232.

[14] M. C. Aragoni, M. Arca, F. A. Devillanova, F. Isaia, V. Lippolis, A. Mancini, L. Pala, A. M. Z. Slawin, J. D. Woollins, *Chem. Commun.* **2003**, 2226–2227.

[15] K. F. Tebbe, R. Buchem, *Angew. Chem.* **1997**, *109*, 1403–1405; *Angew. Chem. Int. Ed. Engl.* **1997**, *36*, 1345–1346.

[16] M. C. Aragoni, M. Arca, F. A. Devillanova, M. B. Hursthouse, S. L. Huth, F. Isaia, V. Lippolis, A. Mancini, *CrystEngComm* **2004**, *6*, 540–542.

[17] T. A. Logothetis, F. Meyer, P. Metrangolo, T. Pilati, G. Resnati, *New J. Chem.* **2004**, *28*, 760–763.

[18] R. Mariaca, G. Labat, N. R. Behrnd, M. Bonin, F. Helbling, P. Eggli, G. Couderc, A. Neels, H. Stoeckli-Evans, J. Hulliger, *J. Fluorine Chem.* **2009**, *130*, 175–196.

[19] B. S. Pedersen, S. Scheibye, N. H. Nilsson, S. O. Lawesson, *Bull. Soc. Chim. Belg.* **1978**, *87*, 223–228.

[20] M. C. Aragoni, M. Arca, F. Demartin, F. A. Devillanova, A. Garau, F. Isaia, F. Lelj, V. Lippolis, G. Verani, *J. Am. Chem. Soc.* **1999**, *121*, 7098–7107.

[21] A. Bittermann, B. Bildstein, K. Wurst, *Z. Kristallogr. New Cryst. Struct.* **2008**, *223*, 231–234.
[22] The carbon–sulfur distance in the second thiocarbonyl group not involved in the CT interactions is almost unaffected compared with those determined for the free donor **4** (**4**·I_2: C5–S5 1.660(14) Å, Figure 2; **4**: 1.662(3) and 1.667(3) Å, Figure 1).
[23] I. L. Karle, *J. Chem. Phys.* **1955**, *23*, 1739–1740.
[24] F. van Bolhuis, P. B. Koster, T. Migehelsen, *Acta Crystallogr.* **1967**, *23*, 90–91.
[25] D. Atzei, P. Deplano, E. F. Trogu, F. Bigoli, M. A. Pellinghelli, A. Sabatini, A. Vacca, *Can. J. Chem.* **1989**, *67*, 1416–1420.
[26] P. H. Svensson, L. Kloo, *Chem. Rev.* **2003**, *103*, 1649–1684.
[27] F. H. Herbstein, W. Schwotzer, *J. Am. Chem. Soc.* **1984**, *106*, 2367–2373.
[28] F. Cristiani, F. Demartin, F. A. Devillanova, F. Isaia, V. Lippolis, G. Verani, *Inorg. Chem.* **1994**, *33*, 6315–6324.
[29] M. C. Aragoni, M. Arca, F. A. Devillanova, F. Isaia, V. Lippolis, *Cryst. Growth Des.* **2012**, *12*, 2769–2779.
[30] V. S. Urusov, I. P. Orlov, *CryRp* **1999**, *44*, 686–760.
[31] M. C. Aragoni, M. Arca, F. Demartin, F. A. Devillanova, F. Lelj, F. Isaia, V. Lippolis, A. Mancini, L. Pala, G. Verani, *Eur. J. Inorg. Chem.* **2004**, 3099–3109.
[32] M. C. Aragoni, M. Arca, F. A. Devillanova, P. Grimaldi, F. Isaia, F. Lelj, V. Lippolis, *Eur. J. Inorg. Chem.* **2006**, 2166–2174.
[33] M. C. Aragoni, M. Arca, F. Demartin, F. A. Devillanova, T. Gelbrich, A. Garau, M. B. Hursthouse, F. Isaia, V. Lippolis, *Cryst. Growth Des.* **2007**, *7*, 1284–1290.
[34] E. J. Juárez-Pérez, M. C. Aragoni, M. Arca, A. J. Blake, F. A. Devillanova, A. Garau, F. Isaia, V. Lippolis, R. Núnez, A. Pintus, C. Wilson, *Chem. Eur. J.* **2011**, *17*, 11497–11514.
[35] F. Isaia, M. C. Aragoni, M. Arca, C. Caltagirone, C. Castellano, F. Demartin, A. Garau, V. Lippolis, A. Pintus, *Dalton Trans.* **2011**, *40*, 4505-4513.
[36] a) A. D. Becke, *J. Chem. Phys.* **1993**, *98*, 5648–5652; b) C. Lee, W. Yang, R. G. Parr, *Phys. Rev. B* **1988**, *37*, 785–789; c) P. J. Stephens, F. J. Devlin, C. F. Chabalowski, M. J. Frisch, *J. Phys. Chem.* **1994**, *98*, 11623–11627.
[37] C. Adamo, V. Barone, *J. Chem. Phys.* **1998**, *108*, 664–675.
[38] S. Grimme, *J. Comput. Chem.* **2006**, *27*, 1787–1799.
[39] Selected optimized metric parameters for **4** (mPW1PW functional; labeling scheme given in Figure 1): C5–S5 1.651, C5–N2 1.390, C5–N1 1.380, C3–C4 1.373, C2–C3 1.451, S1–S2 2.118, S2–S3 2.051, S3–S4 2.118 Å; N1-C5-N2 104.61, C5-N1-C4 110.57, C5-N2-C3 110.54, N2-C3-C4 107.23, N1-C4-C3 107.03, C4-C3-C2-C1 60.11, C26-C21-N2-C3 52.30, C12-C11-N1-C4 64.22°.
[40] Selected natural charges calculated for **4** (mPW1PW functional; labeling scheme given in Figure 1): C5 0.277, N1 −0.454, N2 −0.432, C3 −0.432, C4 0.002, S1 0.148, S2 −0.015, S5 −0.191 *e*.
[41] F. Bigoli, P. Deplano, M. L. Mercuri, M. A. Pellinghelli, E. F. Trogu, A. Vacca, *Phosphorus Sulfur* **1991**, *62*, 53–63.
[42] Selected natural charges calculated for [**4**·I]$^+$ (mPW1PW functional; labeling scheme given in Figure 2): C6 0.332, S6 0.098, I1 0.138, N4 −0.367, N3 −0.383, C2 0.182, C1 0.038, C3 0.103, N1 −0.446, N2 −0.432, C5 0.261, S5 −0.127, S4 0.160, S3 0.023, S2 0.033, S1 0.154 *e*.
[43] a) Selected natural charges calculated for **4**·I_2 (mPW1PW functional; labeling scheme given in Figure 2): C6 0.330, S6 −0.155, I1 −0.050, I2 −0.203, N3 −0.427, N4 −0.408, C1 0.011, C2 0.151, C3 0.138, C4 0.008, N1 −0.453, N2 −0.428, C5 0.274, S5 −0.179, S1 0.148, S2 −0.008, S3 −0.005, S4 0.156 *e*; b) selected natural charges calculated for **4**·2I_2 (mPW1PW functional; labeling scheme given in Figure 2): C6 0.338, S6 −0.154, I1 −0.050, I2 −0.188, N3 −0.427, N4 −0.409, C1 0.018, C2 0.143, S4 0.166, S3 0.002 *e*.
[44] WBIs: I1–I2 0.624, I2···I3 0.237, I3–I4 0.793, I5–I6 0.776.
[45] P. Deplano, F. Devillanova, J. Ferraro, M. L. Mercuri, V. Lippolis, E. F. Trogu, *Appl. Spectrosc.* **1994**, *48*, 1236–1241.
[46] P. Deplano, J. H. Ferraro, M. L. Mercuri, E. F. Trogu, *Coord. Chem. Rev.* **1999**, *188*, 71–95.
[47] Unscaled harmonic frequencies: 173.4, 170.2, 168.9, and 139.2 cm^{-1}; the scaling factor of 0.945 was taken from R. Wysokinski, D. Michalska, *J. Comput. Chem.* **2001**, *22*, 901–912.
[48] a) M. C. Aragoni, M. Arca, F. Demartin, F. A. Devillanova, A. Garau, F. Isaia, V. Lippolis, G. Verani, *Trends Inorg. Chem.* **1999**, *6*, 1–18; b) M. Arca, M. C. Aragoni, F. A. Devillanova, A. Garau, F. Isaia, V. Lippolis, A. Mancini, G. Verani, *Bioinorg. Chem. Appl.* **2006**, 58937.
[49] a) R. H. Blessing, *Acta Crystallogr. Sect. A* **1995**, *51*, 33–37; b) R. H. Blessing, *J. Appl. Crystallogr.* **1997**, *30*, 421–426.
[50] SADABS Area-Detector Absorption Correction Program, Bruker AXS Inc. Madison, WI, USA, **2000**.
[51] A. Altomare, M. C. Burla, M. Camalli, G. L. Cascarano, C. Giacovazzo, A. Guagliardi, A. G. G. Moliterni, G. Polidori, R. Spagna, *J. Appl. Crystallogr.* **1999**, *32*, 115–119.
[52] G. M. Sheldrick, *Acta Crystallogr. Sect. A* **2008**, *64*, 112.
[53] L. J. Farrugia, *J. Appl. Crystallogr.* **1999**, *32*, 837.
[54] Gaussian 09, Revision A02, M. J. Frisch, G. W. Trucks, H. B. Schlegel, G. E. Scuseria, M. A. Robb, J. R. Cheeseman, G. Scalmani, V. Barone, B. Mennucci, G. A. Petersson, H. Nakatsuji, M. Caricato, X. Li, H. P. Hratchian, A. F. Izmaylov, J. Bloino, G. Zheng, J. L. Sonnenberg, M. Hada, M. Ehara, K. Toyota, R. Fukuda, J. Hasegawa, M. Ishida, T. Nakajima, Y. Honda, O. Kitao, H. Nakai, T. Vreven, J. A. Montgomery, Jr., J. E. Peralta, F. Ogliaro, M. Bearpark, J. J. Heyd, E. Brothers, K. N. Kudin, V. N. Staroverov, R. Kobayashi, J. Normand, K. Raghavachari, A. Rendell, J. C. Burant, S. S. Iyengar, J. Tomasi, M. Cossi, N. Rega, J. M. Millam, M. Klene, J. E. Knox, J. B. Cross, V. Bakken, C. Adamo, J. Jaramillo, R. Gomperts, R. E. Stratmann, O. Yazyev, A. J. Austin, R. Cammi, C. Pomelli, J. W. Ochterski, R. L. Martin, K. Morokuma, V. G. Zakrzewski, G. A. Voth, P. Salvador, J. J. Dannenberg, S. Dapprich, A. D. Daniels, Ö. Farkas, J. B. Foresman, J. V. Ortiz, J. Cioslowski, and D. J. Fox, Gaussian, Inc., Wallingford CT, **2009**.
[55] A. Schäfer, H. Horn, R. Ahlrichs, *J. Chem. Phys.* **1992**, *97*, 2571–2577.
[56] a) L. E. Roy, P. J. Hay, R. L. Martin, *J. Chem. Theory Comput.* **2008**, *4*, 1029–1031; b) C. E. Check, T. O. Faust, J. M. Bailey, B. J. Wright, T. M. Gilbert, L. S. Sunderlin, *J. Phys. Chem. A* **2001**, *105*, 8111–8116.
[57] a) A. E. Reed, F. Weinhold, *J. Chem. Phys.* **1983**, *78*, 4066–4073; b) A. E. Reed, R. B. Weinstock, F. Weinhold, *J. Chem. Phys.* **1985**, *83*, 735–746; c) A. E. Reed, L. A. Curtiss, F. Weinhold, *Chem. Rev.* **1988**, *88*, 899–926.
[58] K. Wiberg, *Tetrahedron* **1968**, *24*, 1083–1096.
[59] GaussView, Version 5, R. Dennington, T. Keith, J. Millam, *Semichem Inc.*, Shawnee Mission KS, **2009**.
[60] G. Schaftenaar, J. H. Noordik, *J. Comput.-Aided Mol. Des.* **2000**, *14*, 123–134.
[61] G. Maninchedda, M. Arca, PyFreq, Università degli Studi di Cagliari, **2013**.

Received: May 21, 2013
Published online: September 11, 2013

